MATH 566 - Final Project Report

Md Khorshed Alam

1 INTRODUCTION

The impact of wildfires and post-fire contamination of soil and groundwater has become more pronounced due to the increase in the frequency and intensity of wildfires worldwide. Not only do these fires pose direct hazards, but they can also lead to secondary contamination issues that pose a threat to human and environmental health. For example, the use of aqueous film-forming foams (AFFFs) during fire suppression can release per- and polyfluoroalkyl substances (PFAS) into the soil, which are mobile, toxic, and persist for long periods of time (Ahrens, 2011; Krafft & Riess, 2015; Rayne & Forest, 2009) leading to soil and groundwater contamination. This contamination has mainly affected drinking water and has been linked to a range of human health issues, including complications in fetuses and placentas (Blake & Fenton, 2020; Nian et al., 2020), alterations in baby growth (Liew et al., 2018), and cancer (Vieira et al., 2013), among others (Steenland et al., 2018; Xu et al., 2020).

Despite a significant amount of research in recent years, there is still much that is not known about PFAS, particularly in terms of their behavior in soil and water environments (U.S. EPA, 2021). There is also a limited understanding of how PFAS move and spread in the environment and how they are transported and transformed in different environmental media. This has made it challenging for researchers and regulators to fully assess the risks posed by PFAS and develop effective strategies for managing this family of chemicals.

Recently, Gu et al. (2020) introduced a mathematical model for the transport of PFAS under transient, variably saturated flow in the vadose zone for the first time and implemented this model to a model source zone impacted by AFFF. Later, relying on the mathematical model and experimental data by Gu et al. (2020), Iradukunda and Farid (2022) developed a one-dimensional (1D) Multiphysics numerical model to study the fate and transport of PFAS, incorporating transient seepage and advection-dispersion, also accounting for the adsorption to the air-water interface and solid phase. Both the above-mentioned mathematical and numerical models are limited to analyzing 1D problems and applicable to laboratory scale experiments, whereas a higher-dimensional model is required to investigate more complex and real-world problems.

In the present study, a 2D numerical framework is constructed and numerically solved for PFAS concentration using both direct and iterative solver approaches, namely Gaussian elimination and the generalized minimal residual method (GMRES). Additionally, utilizing the experimental data found in the literature (Guo et al., 2020), various scenarios have been simulated to improve the understanding of PFAS transport in soil environments, taking into

consideration the impacts of advection-dispersion and adsorption to air-water and soil interfaces.

The mathematical formulations, development of the 2D numerical model and the choice of numerical solving methods are discussed in the following section. The simulation results are presented in the results section, followed by a comparative study of both solving approaches for this particular problem.

2 FORMULATION

Various transport processes contribute to the fate and transport of PFAS through soil and groundwater. These transport processes include molecular diffusion, advection, mechanical dispersion, adsorption to the solid phase, and adsorption to air-water interfaces. Mechanical dispersion caused by the advective flow on PFAS through porous media along a tortuous path and molecular diffusion are combined in a term referred to as hydrodynamic dispersion. The latter process of adsorption to the air-water interfaces is relevant to PFAS due to their molecular structure.

The following describes the governing equations of the factors that influence the PFAS transport process.

2.1 Mathematical Formulation

Advection and diffusion are major mechanisms of PFAS flow that can be described by the following equation.

$$\frac{\partial(\theta C)}{\partial t} + \nabla(\theta \boldsymbol{v} C) - \nabla \cdot (\theta \boldsymbol{D} \nabla C) = 0, \quad (1)$$

where C is the aqueous concentration of PFAS (μmol/cm^3); θ is the volumetric water content; $\boldsymbol{v} = q/\theta$ is the interstitial pore-water velocity (cm/s); q is the Darcy flux (cm/s); and $\boldsymbol{D}$ is the dispersion/diffusion coefficient (cm^2/s).

The solid-phase-adsorption term describes the interactions or processes that bind a compound to the surface of the soil. According to Li et al. (2018), PFAS has shown a possible adsorption mechanism due to both electrostatic and hydrophobic interactions. These adsorption mechanisms can be defined by a series of equations quantifying their effects on the overall transport. The solid-phase adsorption can be described using partitioning coefficients such as K_d:

$$K_d = \frac{C_s}{C_{aq}}, \quad (2)$$

where K_d is the partitioning coefficient to the solid phase, C_s is the concentration of the compound adsorbed onto solids, and C_{aq} is the concentration in the solution, in this case, the

aqueous concentration. Depending on the nature and regime governing the adsorption, various models are used. The regime governing the adsorption of PFAS onto the solid phase can be described using a Freundlich isotherm equation as follow.

$$C_s = K_f C^N, \tag{3}$$

where $K_f$and N are fitting parameters found based on experimental data. Therefore, the adsorption onto the solid-phase term of Eq. (4) should be incorporated into the transport equation (Eq. 1).

$$\frac{\partial(\theta C)}{\partial t} + \rho_b \frac{\partial}{\partial t} K_f C^N = 0, \tag{4}$$

where ρ_b is the bulk density of the porous medium (g/cm^3).

Another process that significantly affects the fate and transport of PFAS within the unsaturated zones is the adsorption to air-water interfaces (AWIs) and micelles formation. This is because PFAS acts as a surfactant due to its molecular structure containing a hydrophobic "tail" and hydrophilic "head." Therefore, the adsorption at the air-water interface (Eq. 5) should be incorporated into the transport equation (Eq. 1).

$$\frac{\partial(\theta C)}{\partial t} + \frac{\partial}{\partial t}(A_{aw} K_{aw} C) = 0, \tag{5}$$

where A_{aw} is the air-water interfacial area (cm^2/cm^3); K_{aw} is the air-water interfacial adsorption coefficient (cm^3/cm^2). The air-water interfacial area, A_{aw}, depends on capillary pressure head, water saturation, and the imbibition and drainage history, which can be approximated as a function of water saturation, S_w, as follows (Guo et al., 2020).

$$A_{aw} = x_2 {S_w}^2 + x_1 S_w + x_0, \tag{6}$$

where x_2, x_1, and x_0 are fitting parameters for the soil and sand used in the experiment. Furthermore, the air-water interfacial adsorption coefficient can be described by the following equation (Brusseau, 2018; Kim et al., 1997).

$$K_{aw} = \frac{-1}{RTC}\left(\frac{\partial \sigma}{\sigma \, ln \, C}\right)_T, \tag{7}$$

where the universal gas constant, $R = 8.1314$ JK^{-1} mol^{-1}, T is the temperature (K), and σ is surface tension (dyne/cm), expressed by the Szyszkowski equation, in terms of aqueous concentration C (Chang & Franses, 1995).

$$\sigma = \sigma_0 \left[1 - b \ln\left(1 + \frac{C}{a}\right)\right], \tag{8}$$

where a (μmol/cm^3) and b (-) are fitting parameters to the experimental data. Hence, inserting Equation (7) into Equation (8) yields:

$$K_{aw} = \frac{1}{RT}\frac{\sigma_0 b}{a+C}, \tag{9}$$

which shows that K_{aw} monotonically increases as C decreases and asymptotically approaches a maximum value.

Therefore overall transport of PFAS is governed by the interaction of advection, hydrodynamic diffusion, and adsorption at solid (i.e., soil particles) and air-water interfaces, derived from conservation of mass, described as (Iradukunda & Farid, 2022; Zeng & Guo, 2021):

$$\frac{\partial(\theta C)}{\partial t} + \rho_b \frac{\partial}{\partial t} K_f C^N + \frac{\partial}{\partial t}(A_{aw} K_{aw} C) + \nabla(\theta \boldsymbol{v} C) - \nabla \cdot (\theta \boldsymbol{D} \nabla C) = 0, \tag{10}$$

For a 2D problem, Equation (6) can be written as:

$$\frac{\partial(\theta C)}{\partial t} + F + \frac{\partial}{\partial t}(A_{aw} k_{aw} C) + \frac{\partial}{\partial x}(\theta v_x C) + \frac{\partial}{\partial z}(\theta v_z C) - \frac{\partial}{\partial x}\left(\theta D_x \frac{\partial C}{\partial x}\right) - \frac{\partial}{\partial z}\left(\theta D_z \frac{\partial C}{\partial z}\right) = 0, \tag{11}$$

where $F = \rho_b \frac{\partial}{\partial t} K_f C^N$, and v_x and v_z, and D_x and D_z are components of $\boldsymbol{v}$ and $\boldsymbol{D}$, respectively.

2.2 Numerical framework

A 2D numerical framework was developed using MATLAB to solve the mathematical governing equation (Eq. 11) to outline the conservation of mass. The framework utilized in this paper is a finite-difference method using forward and backward differences for first-order space and time derivatives respectively and central differences for higher-order space derivatives to discretize both the time and space domains. Two types of boundary conditions were considered in the simulation. Most of the boundaries were treated as impermeable boundaries modelled using Neumann boundary conditions, while the inlets and outlets were given constant aqueous concentration values (C_1 and C_2, respectively) using Dirichlet boundary conditions. In order to reduce the computational cost and provide numerical stability of the model, the horizontal grid size (Δx) and the vertical grid size (Δz) at a given time step (Δt) need to follow the mathematical relation below.

$$\Delta x = -D_x \frac{C_2 - C_1}{L}\Delta t, \text{ and } \frac{\Delta x}{\Delta z} = \sqrt{\frac{D_x}{D_z}}, \tag{12}$$

where L is the vertical length of the soil domain. Moreover, relying on the Crank-Nicolson scheme (Chávez-Negrete et al., 2018), concentration C on the right-hand side of Equation (6) for each node is written as the weighted average of the values ${C_{i,j}}^{t+1}$ and ${C_{i,j}}^{t}$ where ${C_{i,j}}^{t}$ is

the concentration of PFAS at Node (i,j). The finite-difference method was used to linearize the governing partial differential equation (PDE) described above (Eq. 11) into Eq. (13).

$$-C_{i,j+1}^{t+1}\left(-\frac{\theta_{i,j}v_{x_{i,j}}}{\Delta x}+\frac{\theta_{i,j}D_{x_{i,j+1}}-\theta_{i,j}D_{x_{i,j}}}{\Delta x^2}+\frac{\theta_{i,j+1}D_{x_{i,j}}}{\Delta x^2}\right)+C_{i,j}^{t+1}\left(\frac{F_{i,j}}{\Delta t}+\frac{A_{aw_{i,j}}K_{aw_{i,j}}}{\Delta t}+\frac{\theta_{i,j}v_{x_{i,j+1}}}{\Delta x}+\right.$$
$$\frac{v_{x_{i,j}}\theta_{i,j+1}}{\Delta x}-3\frac{v_{x_{i,j}}\theta_{i,j}}{\Delta x}+\frac{\theta_{i,j}v_{z_{i+1,j}}}{\Delta y}+\frac{v_{z_{i,j}}\theta_{i+1,j}}{\Delta y}-3\frac{v_{z_{i,j}}\theta_{i,j}}{\Delta y}+\frac{\theta_{i,j}D_{x_{i,j+1}}+\theta_{i,j+1}D_{x_{i,j}}}{\Delta x^2}+$$
$$\left.\frac{\theta_{i,j}D_{y_{i+1,j}}+\theta_{i+1,j}D_{z_{i,j}}}{\Delta y^2}+\frac{\theta_{i,j}}{\Delta t}+\frac{\theta_{i,j}^{t+1}-\theta_{i,j}^{t}}{2\Delta t}+\right)-C_{i+1,j}^{t+1}\left(-\frac{\theta_{i,j}v_{z_{i,j}}}{\Delta y}+\frac{\theta_{i+1,j}D_{z_{i,j}}}{\Delta y^2}+\frac{\theta_{i,j}D_{z_{i+1,j}}-\theta_{i,j}D_{z_{i,j}}}{\Delta y^2}\right)-$$
$$C_{i,j-1}^{t+1}\left(\frac{\theta_{i,j}D_{x_{i,j}}}{\Delta x^2}\right)-C_{i-1,j}^{t+1}\left(\frac{\theta_{i,j}D_{z_{i,j}}}{\Delta y^2}\right)=C_{i,j}^{t}\left(\frac{F_{i,j}}{\Delta t}+\frac{A_{aw_{i,j}}K_{aw_{i,j}}}{\Delta t}+\frac{\theta_{i,j}}{\Delta t}-\frac{\theta_{i,j}^{t+1}-\theta_{i,j}^{t}}{2\Delta t}\right), \quad (13)$$

where the Crank-Nicolson schema was used over each time step, i.e., $\theta_{i,j}=\frac{\theta_{i,j}^{t+1}+\theta_{i,j}^{t}}{2}$, $D_{i,j}=\frac{D_{i,j}^{t+1}+D_{i,j}^{t}}{2}$, and $A_{aw_{i,j}}=\frac{A_{aw}{}_{i,j}^{t+1}+A_{aw}{}_{i,j}^{t}}{2}$.

However, coefficients F and K_{aw} are nonlinear functions of C. To maintain the linearity of the discretized equation (Eq. 13), F and $K_{aw}$are updated using a successive iteration scheme. Basically, starting with an initial value of ${C_{i,j}}^{t}$, $F_{i,j}^{t}$ and $K_{aw}{}_{i,j}^{t}$ are computed using to initiate a time step to determine ${C_{i,j}}^{t+1}$, and prior to proceeding to the next time step, a successive iteration scheme is employed to update the values of $F_{i,j}^{t}$ and $K_{aw}{}_{i,j}^{t}$, until convergence to the optimal F_i^{t+1} and $K_{aw}{}_i^{t+1}$. This guarantee maintaining the linearity of Eq. (13). This allows for solving the system of linear equations presented by Eq. (11). At the subsequent time step, C_i^{t+2} is calculated based on the average values of F and K_{aw} at time $t+1$ and t, and another successive iteration continues until converges to the best F_i^{t+2}, and $K_{aw}{}_i^{t+2}$. This process will repeat until the final time.

2.3 Numerical methods

To investigate this 2D problem, we use a MATLAB built-in direct numerical solver method called the Gaussian elimination method (GEM) since the considered matrix is moderately sized and has a favorable sparsity pattern. Moreover, GEM computes exact solutions to the system of linear equations as long as the matrix is well-conditioned, and the elimination process is carried out correctly. The computational cost of Gaussian elimination is typically $O(n^3)$, where n is the number of unknowns. In this problem, we are solving for C is the aqueous concentration of PFAS, which is of size $P\times 1$, where $P=18\times 14=216$ therefore computational cost should be $O(P^3)$. However, the original cost might be less as GEM could take the advantage of the sparsity of the coefficient matrix.

On the other hand, an iterative numerical scheme known as Generalized Minimal Residual method (GMRES) was also implemented to solve this system, which turns out to be more computationally expensive than GEM for this particular problem. A comparative performance study between these solving approaches is outlined in the result section.

2.4 Experimental data and parameters

The model is designed in such a manner that it allows for the investigation of PFAS transport through diverse soil types and various scenarios. In this study, the transport of PFAS is simulated through Accusand soil, and for this simulation, the necessary data and parameters were obtained from a study conducted by Guo et al. (2020).

Table 1. *A summary of the parameters that are used in the simulations for Accusand soil.*

Parameter	Value	Unit
$\boldsymbol{\rho_b}$	1.65	g/cm^3
$\boldsymbol{K_f}$	0.055	(µmol/g)/(µmol/cm^3)^N
$\boldsymbol{N}$	0.85	-
$\boldsymbol{\sigma}$	71	dyne/cm
$\boldsymbol{R}$	8.314	J/K/mol
$\boldsymbol{T}$	293.15	K
$\boldsymbol{a}$	0.004	µmol/cm^3
$\boldsymbol{b}$	0.017	-
$\boldsymbol{x_2}$	548.54	-
$\boldsymbol{x_1}$	-1182.5	-
$\boldsymbol{x_0}$	633.96	-

2.5 Problem setup

The overall transport Eq. (11) was simulated based on two types of boundary conditions. Neumann boundary conditions are considered at all boundaries except for the inlet and outlets. Dirichlet boundary conditions were considered at the inlet and outlets. A constant supply of PFAS concentration is simulated at the inlet on the mid-point on the left vertical boundary. Outlets are considered exposed to an abundance of freshwater; hence, no accumulation of PFAS occurs at three outlets (end corners and mid- point) on the right vertical boundary. It was assumed that there is no initial PFAS contaminant in soil. Therefore, at all the nodes on the mesh grid the concentration of PFAS is 0. Then, for the first-time step, PFAS was introduced at the inlet with a concentration of 12 µmol/cm^2. Neumann boundary conditions allowed us to simulate the transport of PFAS assuming there is a constant supply of PFAS at the inlet and an accumulation of PFAS concentration at outlets allowing breakthrough concentration.

The following is considered for all of the cases of simulations: (i) initially, the concentration of PFAS in the soil is $C = 0$ µmol/cm^2; (ii) except for the inlet and outlets, all other boundaries of soil are impermeable; (iii) the concentration of PFAS at the inlet $C_1 = 12$ mg/L and at outlets $C_2 = 0$ mg/L, for all time steps; (iv) time step size $\Delta t = 5$ seconds; (v) the soil sample size horizontal length $L = 2.1$ m and vertical length (thickness) $H = 2$ m; (vi) the components of the diffusion coefficient $\boldsymbol{D}$ have values $D_x = 5.5 \times 10^{-3}$ m^2/s and $D_z = 1.5 \times 10^{-3}$ m^2/s (D_{xz} = 0 m^2/s); (vii) soil porosity $n = 0.00294$.

3 RESULTS AND DISCUSSION

3.1 Simulation results

Based on the data presented in the previous section, several scenarios have been numerically simulated for a soil sample with domain discretized into a 18×14 grid, to analyze the impact on PFAS transport due to diffusion, advection, and adsorption onto the air-water and solid-phase interfaces.

The results are demonstrated as snapshots in time of the spatial distribution of PFAS concentration and the time history at specific locations (i.e., node numbers). Time histories are shown for three nodes, one immediately after (to the right) of the inlet, referred to as the "Start point," a node just before the outlet at the mid-vertical level, referred to as the "Endpoint," and a node at the center of the grid referred to as "Midpoint."

3.1.1 Effect of diffusion coefficients on the transport of PFAS

To investigate the individual effect of diffusion coefficients on the transport of PFAS through fully saturated soil, other terms (e.g. advection, and adsorption onto the air-water and solid-phase interfaces) in Equation (8), were disregarded, and the governing equation would be as follows. This case is analyzed for a water-saturated case ($S_w = 1$).

$$\frac{\partial(\theta C)}{\partial t} - \left(\theta D_x \frac{\partial C}{\partial x}\right) - \frac{\partial}{\partial z}\left(\theta D_z \frac{\partial C}{\partial z}\right) = 0. \tag{14}$$

The following figures show a snapshot of the spatial distribution after 12000 sec (3 hours and 20 min), and the time history of PFAS transportation.

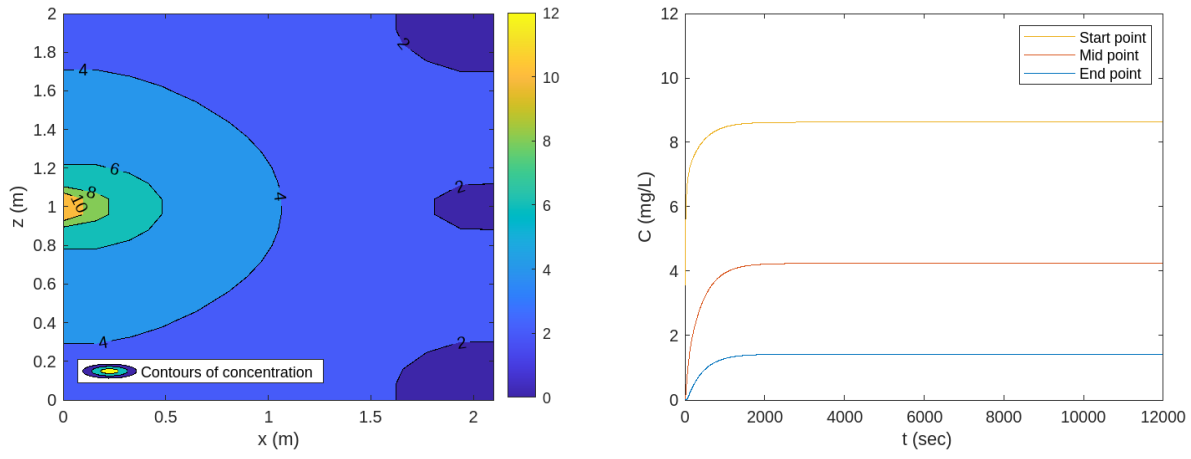

(a) (b)

Figure 1. *Diffusion due to a constant supply of PFAS at inlet on the left boundary and three outlets on the right boundary exposed to an abundance of freshwater considering: (a) spatial distribution at time t =12000 seconds; (b) time history of PFAS transportation at three nodes over time.*

3.1.2 Effect of advection-diffusion coefficients on the transport of PFAS

In this scenario, the advection term is introduced in addition to the diffusion coefficients, and the governing equation takes the following form.

$$\frac{\partial(\theta C)}{\partial t} + \frac{\partial}{\partial x}(\theta v_x C) + \frac{\partial}{\partial z}(\theta v_z C) - \left(\theta D_x \frac{\partial C}{\partial x}\right) - \frac{\partial}{\partial z}\left(\theta D_z \frac{\partial C}{\partial z}\right) = 0. \quad (15)$$

To analyze advection and visualize its effect on PFAS transportation, two values of flow velocity, $\boldsymbol{v}$ are used: (i) $v_x = 1 \times 10^{-3}$ cm/s and $v_z = 0$ cm/s and (ii) $v_x = 3 \times 10^{-3}$ cm/s and $v_z = 0$ cm/s. This case is analyzed for a water-saturated case ($S_w = 1$) .

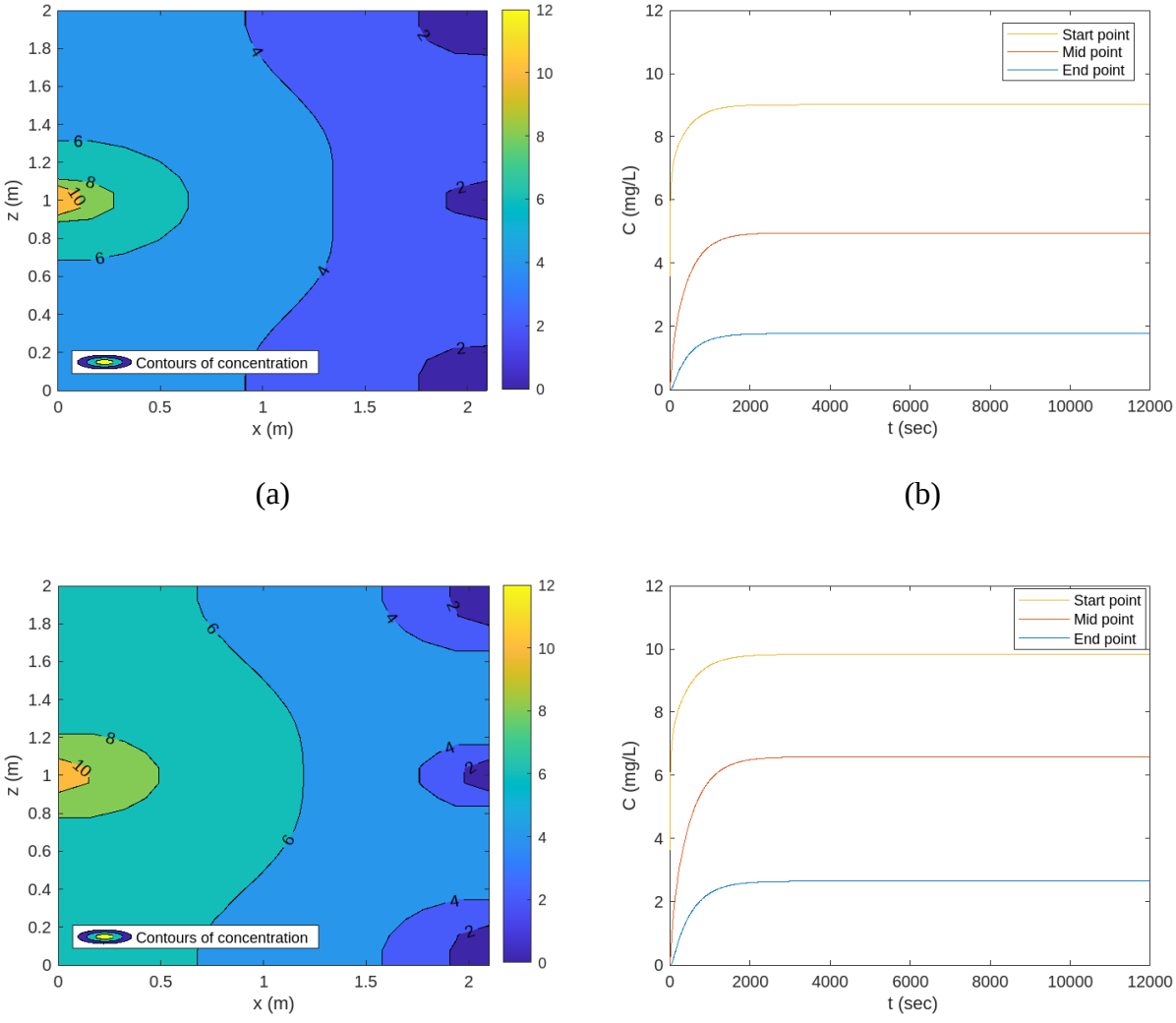

Figure 2. *Diffusion and advection due to a constant supply of PFAS at inlet on the left boundary and three outlets on the right boundary exposed to an abundance of freshwater considering: (a) spatial distribution at time t =12000 seconds for* ***Scenario 1 ($v_x = 1 \times 10^{-3}$ cm/s)****; (b) time history of PFAS transportation at three nodes over time for* ***Scenario 1 ($v_x = 1 \times 10^{-3}$ cm/s)****; (c) spatial distribution at time t =12000 seconds for* ***Scenario 2 ($v_x = 3 \times 10^{-3}$ cm/s)****; (d) time history of PFAS transportation at three nodes over time for* ***Scenario 2 ($v_x = 3 \times 10^{-3}$ cm/s)****.*

3.1.3 Effect of adsorption onto solid-phase interfaces on the transport of PFAS

Adding the terms $F = \rho_b \frac{\partial}{\partial t} K_f C^N$ will introduce the adsorption onto solid-phase interfaces into Eq. (15):

$$\frac{\partial(\theta C)}{\partial t} + F + \frac{\partial}{\partial x}(\theta v_x C) + \frac{\partial}{\partial z}(\theta v_z C) - \frac{\partial}{\partial x}\left(\theta D_x \frac{\partial C}{\partial x}\right) - \frac{\partial}{\partial z}\left(\theta D_z \frac{\partial C}{\partial z}\right) = 0. \quad (16)$$

In this case, flow velocity v with components $v_x = 3 \times 10^{-3}$ cm/s and $v_z = 0$ cm/s was taken into consideration. The resulting two cases demonstrate the impact of solid-phase adsorption on PFAS diffusion (no advection). Two values were selected K_f: $K_f = 0.055$ µmol/g from the experimental data and a choice with less adsorptive nature, $K_f = 0.01$ µmol/g. This case is analyzed for a water-saturated condition ($S_w = 1$).

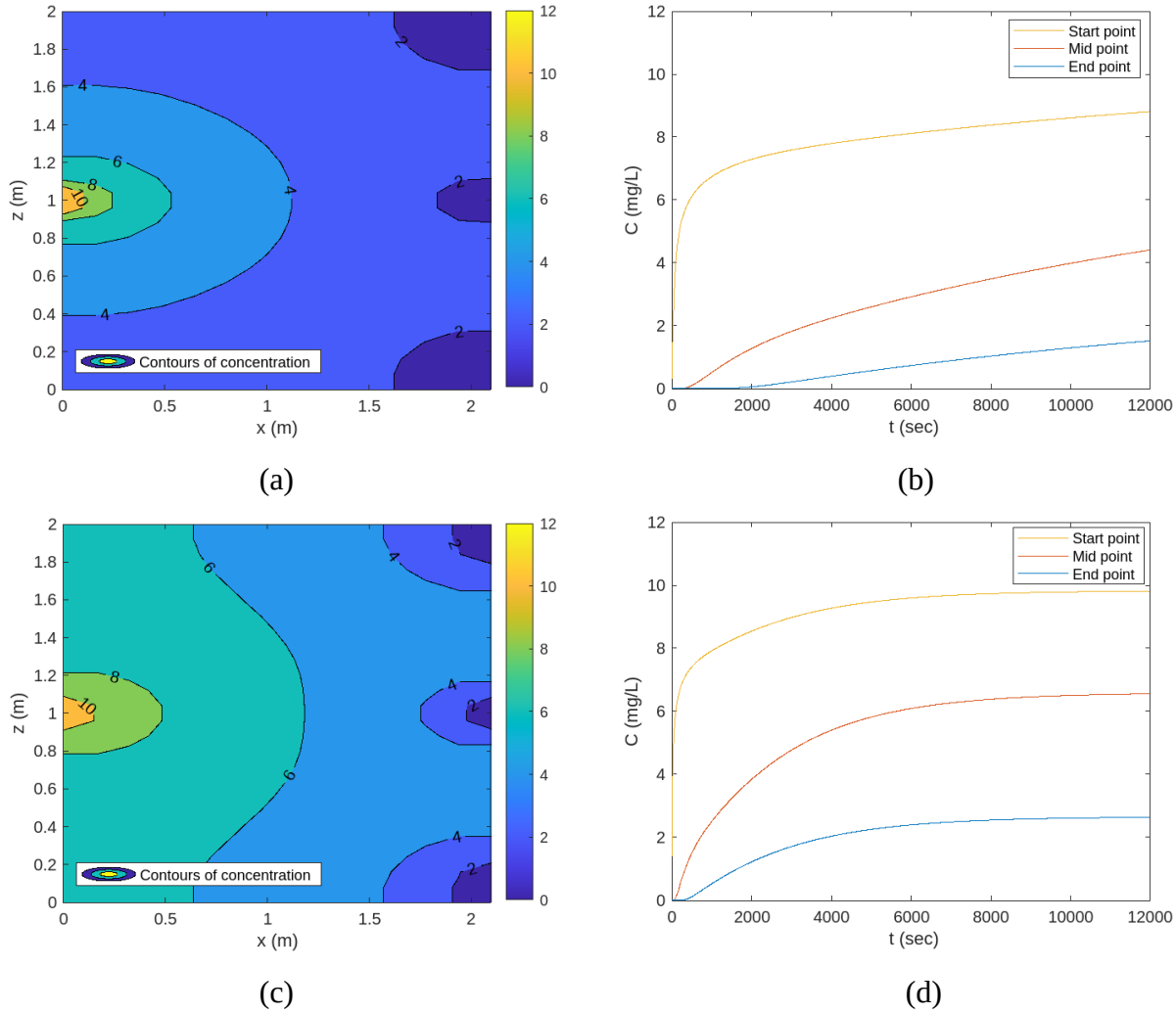

Figure 3. *Diffusion and adsorption to soil, a constant supply of PFAS at inlet on the left boundary and three outlets on the right boundary exposed to an abundance of freshwater considering: (a) spatial distribution at time t =12000 seconds for* ***Scenario 1 ($K_f = 0.055$ µmol/g)****; (b) time history of PFAS transportation at three nodes over time for* ***Scenario 1 ($K_f = 0.055$ µmol/g)****; (c) spatial distribution at time t =12000 seconds for* ***Scenario 2 ($K_f = 0.01$***

µmol/g); *(d) time history of PFAS transportation at three nodes over time for* ***Scenario 2 (K_f = 0.01 µmol/g)***.

3.1.4 Effect of adsorption onto air-water interfaces on the transport of PFAS

Finally, considering the adsorption on air-water interfaces, Equation (16) turns into the following equation which represent the overall PFAS transport.

$$\frac{\partial(\theta C)}{\partial t} + F + \frac{\partial}{\partial t}(A_{aw}k_{a\omega}C) + \frac{\partial}{\partial x}(\theta v_x C) + \frac{\partial}{\partial z}(\theta v_z C) - \frac{\partial}{\partial x}\left(\theta D_x \frac{\partial C}{\partial x}\right) - \frac{\partial}{\partial z}\left(\theta D_z \frac{\partial C}{\partial z}\right) = 0. \quad (17)$$

Results are shown for diffusion and adsorption to air-water interface for air content of 0%, 45%, and 90%, flow velocity components $v_x = 3 \times 10^{-3}$ cm/s, $v_z = 0$ cm/s and for K_f = 0.01 µmol/g.

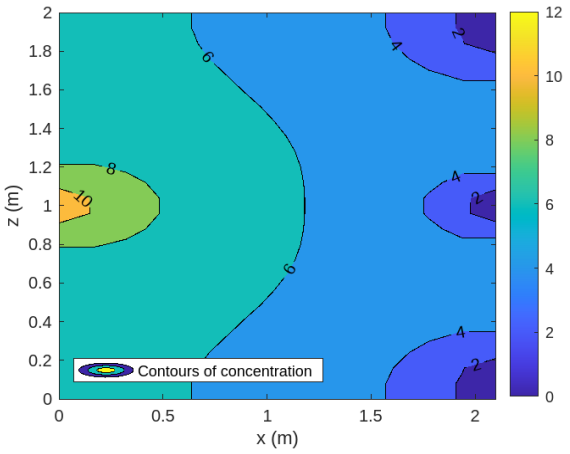

(a)

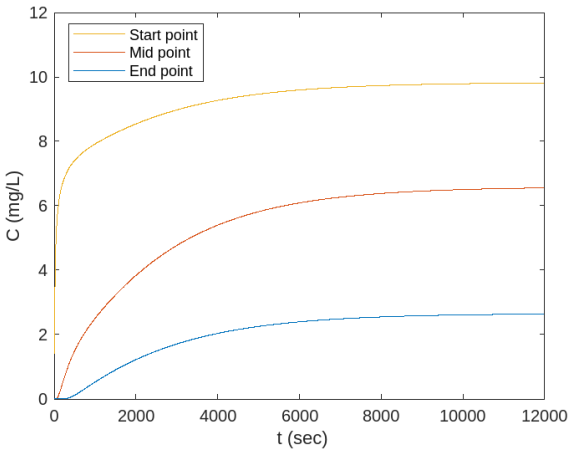

(b)

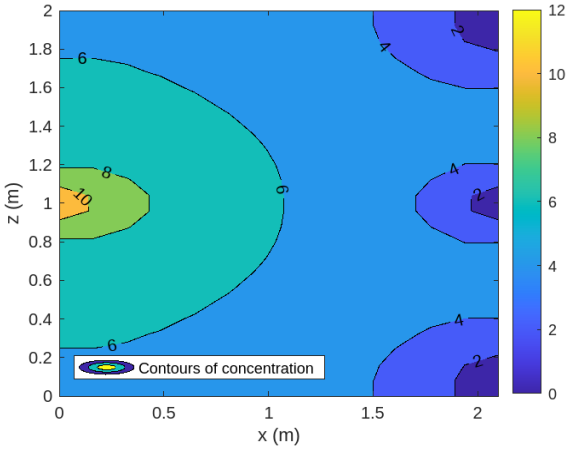

(c)

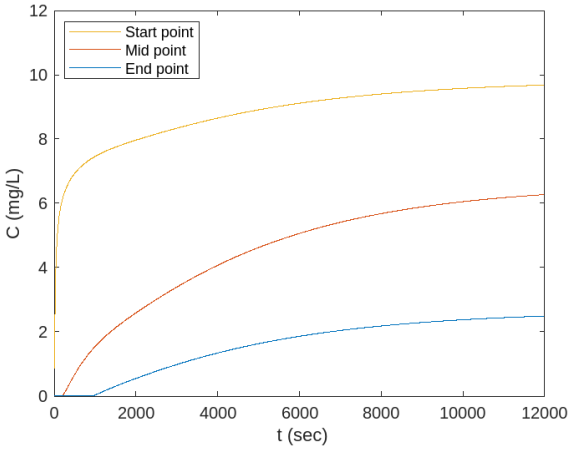

(d)

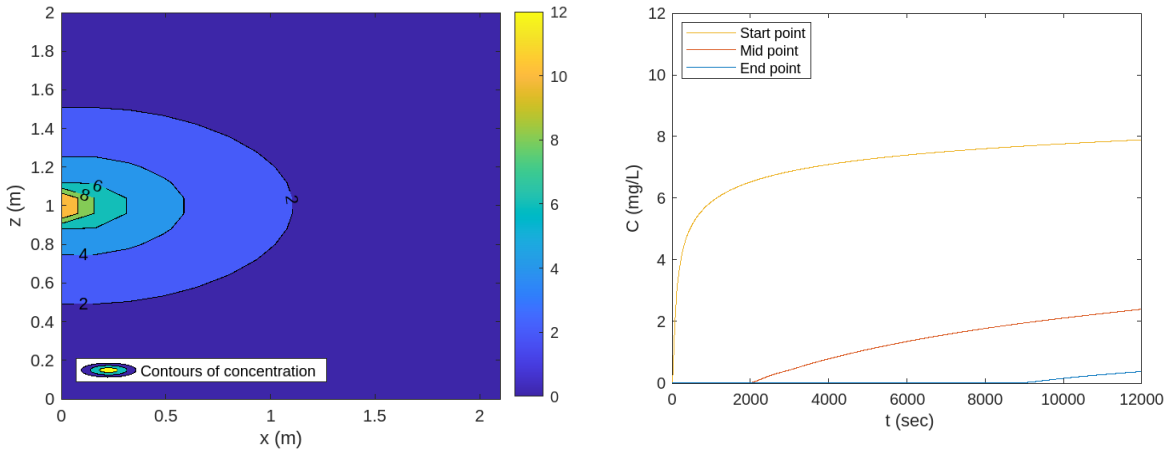

(e) (f)

Figure 4. *Diffusion due to a constant supply of PFAS at inlet on the left boundary and three outlets on the right boundary exposed to an abundance of freshwater considering: (a) spatial distribution at time t=30000 seconds for* ***Scenario 1 ($A_{air} = 0$, $S_{water} = 1$)****; (b) time history of PFAS transportation at three nodes over time for* ***Scenario 1 ($A_{air} = 0$, $S_{water} = 1$)****; (c) spatial distribution at time t =12000 seconds for* ***Scenario 2 ($A_{air} = 0.45$, $S_{water} = 0.55$)****; (d) time history of PFAS transportation at three nodes over time for* ***Scenario 2 ($A_{air} = 0.45$, $S_{water} = 0.55$)*** *(e) spatial distribution at time t =12000 seconds for* ***Scenario 3 ($A_{air} = 0.9$, $S_{water} = 0.1$)****; (f) time history of PFAS transportation at three nodes over time for* ***Scenario 3 ($A_{air} = 0.9$, $S_{water} = 0.1$).***

3.2 Comparison between direct and iterative numerical methods

To compare computational efficiency between the direct numerical scheme GEM and the iterative numerical scheme GMRES, Eqs. (14) – (17) were solved again using the GMRES method for various time step sizes with tolerance 10^{-12}. Table 2 shows the computational time taken for both the GEM and GMRES methods for diffusion and advection-diffusion transport processes, respectively.

Table 2. *Comparison computational time (sec) between GEM and GMRES for diffusion(left) and advection-diffusion (right).*

Δt (sec)	Computational time (sec)	
	GEM	GMRES
10	0.626416	4.559691
9	0.977405	6.617917
8	1.49206	8.453158
6	2.231077	13.77544
5	3.376283	20.65561
4	5.632207	32.48154
3	12.34209	47.18919
2	47.2872	151.6171

Δt (sec)	Computational time (sec)	
	GEM	GMRES
10	0.612292	4.39463
9	0.901113	6.628201
8	1.31957	8.536424
6	2.271031	14.366456
5	3.182209	18.373707
4	5.544346	29.962961
3	12.633138	48.765408
2	42.025024	169.073177

The following Figure 5 is the log-log scale plot based on the data presented in Table 2.

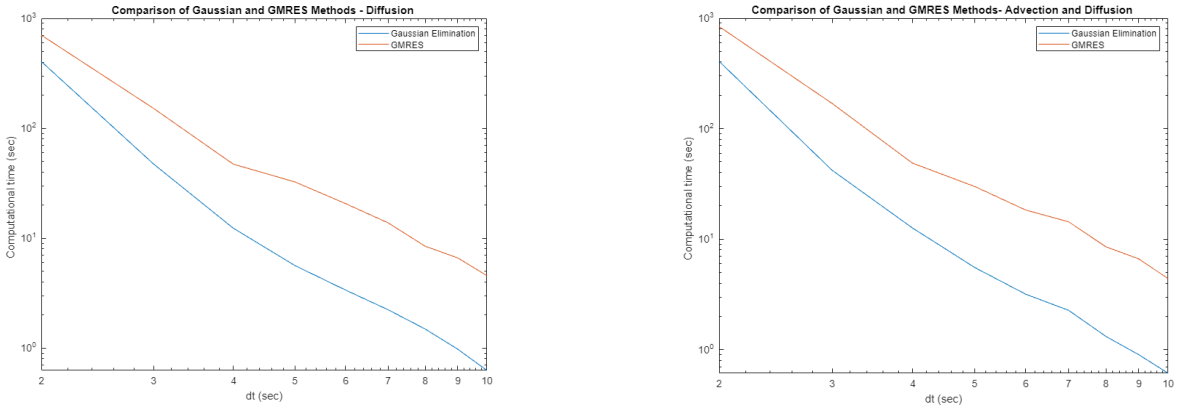

(a) (b)

Figure 5. *Log-log scale plot of taken computational time in seconds by Gaussian elimination method and Generalized minimal residual methods for t time step size $\Delta t = 2$ sec to 10 sec considering: (a) diffusion and (b) advection-diffusion.*

3.3 Discussion on simulation results and performance of numerical methods

Above simulation results demonstrate the relative importance of different transport mechanisms on PFAS movement. The impact of diffusion on the PFAS transport process and the temporal evolution at specified points are depicted in Figure 1. As expected, the transport of PFAS speeds up as soon as advection is introduced, as shown in Figure 2. As seen this faster transport is more pronounced for higher water flow flux. Figure 3 demonstrates that the transport process is retarded when adsorption onto the solid phase is introduced. The transport is more retarded for more adsorptive cases (higher K_f). Finally, Figure 4 shows that with the introduction of more air into the saturated soil, PFAS transport is retarded more.

Nevertheless, the dominant controlling factor for the movement of PFAS in saturated systems depends on the specific conditions of the system. In general, advection tends to be the dominant factor for PFAS transport in saturated systems. However, the presence of adsorption or air in the soil can significantly impact PFAS transport rates and can become the dominant factor in unsaturated systems. Therefore, it is important to consider all of the relevant factors when analyzing PFAS transport in a specific system.

However, Table 2 and Figure 5 show that GEM consistently outperformed GMRES for this system when it came to transport processes like diffusion and advection-diffusion. If we also take into account the solid-phase adsorption and air-water adsorption transport systems, we find a similar trend in computational time. Additionally, it was noticed that the GMRES method wasn't converging for any time step size of $\Delta t < 8$ seconds when solid-phase adsorption with tolerance 10^{-12} was taken into consideration.

The superior performance of GEM in this instance could be attributed to a number of factors. For instance, GMRES is frequently combined with preconditioning techniques to hasten convergence. However, the preconditioning process can be time-consuming, and the choice of preconditioner can be problem dependent. GEM, on the other hand, doesn't need preconditioning and can be straightforward to implement. On top of that, because the system resulting from the PDE is sparse, GEM typically requires fewer operations than GMRES. Additionally, depending on the system, GMRES may need more iterations to converge, whereas Gaussian elimination offers exact solutions without requiring iterations.

4 CONCLUSIONS

A two-dimensional (2D) numerical model is presented in this paper to simulate the transport of PFAS. The model's details were covered, and a range of results for various scenarios was exhibited to demonstrate the effects of diffusion, advection, and adsorption onto solid-phase and air-water interfaces at various air contents. The transport of PFAS is observed to accelerate significantly upon the introduction of advection, a mechanism that tends to exert dominant control over the transport process. Conversely, the transport process experiences retardation upon the addition of air, which leads to increased adsorption of PFAS onto the soil. Moreover, this study shows that for both individual and overall PFAS transport processes, the direct numerical approach Gaussian elimination method excelled over the iterative solver Generalized minimal residual method.

The numerical model employed in this study offers a quantitative approach to analyzing these factors and their relative contributions to PFAS transport. Furthermore, the comparison between direct and iterative approaches gives us insights into choosing suitable methods for similar types of problems.

REFERENCES

Ahrens, L. (2011). Polyfluoroalkyl compounds in the aquatic environment: A review of their occurrence and fate. *Journal of Environmental Monitoring: JEM*, *13*(1), 20–31. https://doi.org/10.1039/c0em00373e

Blake, B. E., & Fenton, S. E. (2020). Early life exposure to per- and polyfluoroalkyl substances (PFAS) and latent health outcomes: A review including the placenta as a target tissue and possible driver of peri- and postnatal effects. *Toxicology*, *443*, 152565. https://doi.org/10.1016/j.tox.2020.152565

Brusseau, M. L. (2018). Assessing the potential contributions of additional retention processes to PFAS retardation in the subsurface. *Science of The Total Environment*, *613–614*, 176–185. https://doi.org/10.1016/j.scitotenv.2017.09.065

Chang, C.-H., & Franses, E. I. (1995). Adsorption dynamics of surfactants at the air/water interface: A critical review of mathematical models, data, and mechanisms. *Colloids and Surfaces A: Physicochemical and Engineering Aspects*, *100*, 1–45. https://doi.org/10.1016/0927-7757(94)03061-4

Chávez-Negrete, C., Domínguez-Mota, F. J., & Santana-Quinteros, D. (2018). Numerical solution of Richards' equation of water flow by generalized finite differences. *Computers and Geotechnics*, *101*, 168–175. https://doi.org/10.1016/j.compgeo.2018.05.003

Guo, B., Zeng, J., & Brusseau, M. L. (2020). A Mathematical Model for the Release, Transport, and Retention of Per- and Polyfluoroalkyl Substances (PFAS) in the Vadose Zone. *Water Resources Research*, *56*(2), e2019WR026667. https://doi.org/10.1029/2019WR026667

Iradukunda, P., & Farid, A. (2022). *Multiphysics Numerical Modeling of Transient Transport of PFAS*. 149–158. https://doi.org/10.1061/9780784484050.016

Kim, H., Rao, P. S. C., & Annable, M. D. (1997). Determination of effective air-water interfacial area in partially saturated porous media using surfactant adsorption. *Water Resources Research*, *33*(12), 2705–2711. https://doi.org/10.1029/97WR02227

Krafft, M. P., & Riess, J. G. (2015). Per- and polyfluorinated substances (PFASs): Environmental challenges. *Current Opinion in Colloid & Interface Science*, *20*(3), 192–212. https://doi.org/10.1016/j.cocis.2015.07.004

Li, Y., Oliver, D., & Kookana, R. (2018). A critical analysis of published data to discern the role of soil and sediment properties in determining sorption of per and polyfluoroalkyl substances (PFASs). *Science Of the Total Environment*, *628-629*, 110-120. https://doi.org/10.1016/j.scitotenv.2018.01.167

Liew, Z., Goudarzi, H., & Oulhote, Y. (2018). Developmental Exposures to Perfluoroalkyl Substances (PFASs): An Update of Associated Health Outcomes. *Current Environmental Health Reports*, *5*(1), 1–19. https://doi.org/10.1007/s40572-018-0173-4

Nian, M., Luo, K., Luo, F., Aimuzi, R., Huo, X., Chen, Q., Tian, Y., & Zhang, J. (2020). Association between Prenatal Exposure to PFAS and Fetal Sex Hormones: Are the Short-Chain PFAS Safer? *Environmental Science & Technology*, *54*(13), 8291–8299. https://doi.org/10.1021/acs.est.0c02444

Rayne, S., & Forest, K. (2009). Perfluoroalkyl sulfonic and carboxylic acids: A critical review of physicochemical properties, levels and patterns in waters and wastewaters, and treatment methods. *Journal of Environmental Science and Health. Part A, Toxic/Hazardous Substances & Environmental Engineering*, *44*(12), 1145–1199. https://doi.org/10.1080/10934520903139811

Steenland, K., Kugathasan, S., & Barr, D. B. (2018). PFOA and ulcerative colitis. *Environmental Research*, *165*, 317–321. https://doi.org/10.1016/j.envres.2018.05.007

US EPA, O. (2021, October 15). *Increasing Our Understanding of the Health Risks from PFAS and How to Address Them* [Overviews and Factsheets]. https://www.epa.gov/pfas/increasing-our-understanding-health-risks-pfas-and-how-address-them

Vieira, V. M., Hoffman, K., Shin, H.-M., Weinberg, J. M., Webster, T. F., & Fletcher, T. (2013). Perfluorooctanoic acid exposure and cancer outcomes in a contaminated community: A geographic analysis. *Environmental Health Perspectives*, *121*(3), 318–323. https://doi.org/10.1289/ehp.1205829

Xu, Y., Li, Y., Scott, K., Lindh, C. H., Jakobsson, K., Fletcher, T., Ohlsson, B., & Andersson, E. M. (2020). Inflammatory bowel disease and biomarkers of gut inflammation and permeability in a community with high exposure to perfluoroalkyl substances through drinking water. *Environmental Research*, *181*, 108923. https://doi.org/10.1016/j.envres.2019.108923

Zeng, J., & Guo, B. (2021). Multidimensional simulation of PFAS transport and leaching in the vadose zone: Impact of surfactant-induced flow and subsurface heterogeneities. *Advances in Water Resources*, *155*, 104015. https://doi.org/10.1016/j.advwatres.2021.104015

APPENDIX

- Numerical framework developed using MATLAB interface,
  - Comprises 13 MATLAB scripts and functions.
- Execution of "main.m" script to demonstrate simulations.
- Usage of program explained in README file.
- Accessible on GitHub.